Modeling of wave propagation in drill strings using vibration transfer matrix methods

Je-Heon Han and Yong-Joe Kim[a)]

Acoustics and Signal Processing Laboratory, Department of Mechanical Engineering, Texas A&M University,
3123 TAMU, College Station, Texas 77843-3123

Mansour Karkoub

Department of Mechanical Engineering, Texas A&M University at Qatar,
Texas A&M Engineering Building, P.O. Box 23874, Doha, Qatar

In order to understand critical vibration of a drill bit such as stick-slip and bit-bounce and their wave propagation characteristics through a drill string system, it is critical to model the torsional, longitudinal, and flexural waves generated by the drill bit vibration. Here, a modeling method based on a vibration transfer matrix between two sets of structural wave variables at the ends of a constant cross-sectional, hollow, circular pipe is proposed. For a drill string system with multiple pipe sections, the total vibration transfer matrix is calculated by multiplying all individual matrices, each is obtained for an individual pipe section. Since drill string systems are typically extremely long, conventional numerical analysis methods such as a finite element method (FEM) require a large number of meshes, which makes it computationally inefficient to analyze these drill string systems numerically. The proposed "analytical" vibration transfer matrix method requires significantly low computational resources. For the validation of the proposed method, experimental and numerical data are obtained from laboratory experiments and FEM analyses conducted by using a commercial FEM package, ANSYS. It is shown that the modeling results obtained by using the proposed method are well matched with the experimental and numerical results.
© 2013 Acoustical Society of America. [http://dx.doi.org/10.1121/1.4816539]

I. INTRODUCTION

A modeling method for predicting structural waves propagating in a drill system is proposed in this article. The proposed method is based on a vibration transfer matrix approach in which a constant cross-sectional drill pipe section is modeled by using an "analytical" vibration transfer matrix between two sets of structural wave variables at the two ends of the pipe section. For a drill pipe system with multiple cross-sectional pipe sections, multiple transfer matrices, of which each represents one constant pipe section, are obtained. The total transfer matrix of this multi-cross-sectional drill pipe system is then obtained by multiplying all of the individual transfer matrices. Thus, after this matrix multiplication, only two sets of variables at the two ends of the multi-cross-sectional pipe system are related by the total transfer matrix as the final form of the model equation.

Drumheller *et al.* investigated longitudinal waves propagating in a drill pipe system by using a finite difference method (FDM).[1] Wang *et al.*[2] applied a vibration transfer matrix method to predict longitudinal waves in a drill pipe system and compared their results to the FDM results in Ref. 1. However, they investigated the only longitudinal wave case, where a 2×2 transfer matrix is used to describe the wave motion in a drill pipe section.

Torsional vibration such as stick-slip vibration is considered to be one of the most common causes for drill-string system failures. Even low-level, stick-slip vibration can be a major cause of bit wear and reduce the speed of penetration.[3] Axial vibration (i.e., longitudinal vibration) resulted from the interaction between a drill bit and a well bottom can cause a bit-bounce. This may result in a large fluctuation of a weight on bit and thus may damage the tool face of the drill bit and cause poor directional control.

In order to investigate and prevent these critical vibrations, all of the flexural (i.e., lateral), torsional, and longitudinal (i.e., axial) vibration modes of a drill string system should be considered. In this article, a vibration transfer matrix method to model all of the three vibration modes in terms of their wave propagation characteristics is proposed, while the longitudinal vibration is only considered in Refs. 1 and 2. Although various transfer matrix methods have been widely used to determine the acoustic characteristics of many vibro-acoustic systems such as silencers[4] and poroelastic materials,[5] a complete vibration transfer function including all of the three structural waves in drill string systems has not been reported before.

Here, a vibration transfer matrix from longitudinal, torsional, flexural wave equations is first derived based on the assumption that these waves are uncoupled. However, in a real drill pipe system, these waves are weakly coupled through the curvature of the cylinder as well as Poisson's ratio. Therefore, it is required to consider these coupling effects to derive a more accurate "coupled" vibration transfer

[a)]Author to whom correspondence should be addressed. Electronic mail:
joekim@tamu.edu

matrix than the uncoupled one. Then, another vibration transfer matrix is derived by using a thick cylindrical shell model to consider the coupling effects in this article. The vibration transfer matrix derived from the thick cylindrical shell model is reported for the first time to the best of the authors' knowledge.

The proposed transfer matrix approach greatly simplifies modeling procedures and vibration analyses in a computationally-efficient way when compared to other approaches such as a finite element method (FEM) where an extensively large number of finite elements (FEs) are required to model a long pipe system. Since the structural wave variables include forces at a Bottom Hole Assembly (BHA) as well as displacements at ground level, the proposed approach can also be used to analyze the effects of force excitation at the BHA on the vibration of a drill string at the ground level.

The proposed transfer matrices are validated by comparing both the analytical and predicted dispersion curves of a cylindrical pipe. As another validation case, the frequency response functions (FRFs) obtained from the proposed transfer matrices are compared to "experimental" results as well as "numerical" results obtained by using a commercial FEM software package, ANSYS.

II. UNCOUPLED VIBRATION TRANFER MATRIX DERIVED FROM THREE UNCOUPLED WAVE EQUATIONS

An uncoupled vibration transfer matrix that relates structural wave variables between two axial locations in a constant-cross-sectional circular pipe or collar is derived from three uncoupled wave equations. These uncoupled wave equations describe the longitudinal, torsional, and flexural waves propagating in the pipe or collar. The structural wave variables used for this transfer matrix description is defined in Fig. 1. For convenience, the subscript "1" means the variables at $z = 0$ and the subscript "2" represents the variables at $z = L$.

A. Longitudinal wave

For the system shown in Fig. 1, the longitudinal wave equation[6] can be represented as

$$\frac{\partial^2 u_z}{\partial z^2} = \frac{1}{c_L^2} \frac{\partial^2 u_z}{\partial t^2}, \tag{1}$$

where u_z is the longitudinal displacement in the z-direction [see Fig. 1(a)], c_L is the longitudinal wave speed defined as $c_L = (E/\rho)^{1/2}$, E is the Young's modulus, and ρ is the density. The longitudinal wave solution for Eq. (1) can then be assumed as

$$u_z = (Ce^{ik_L z} + De^{-ik_L z})e^{-i\omega t}, \tag{2}$$

where ω is the angular frequency and k_L is the longitudinal wave number defined as

$$k_L = \frac{\omega}{c_L}. \tag{3}$$

In the solution of Eq. (2), it is assumed that only plane wave is propagating through the drill pipe section, which is valid in low frequencies where higher cross-sectional wave modes decay out exponentially and can thus be negligible. Most of the drill string failures occur in this low frequency range. By plugging the wave solution of Eq. (2) into the longitudinal wave equation and using the axial force and displacement relation, $N_{zz} = -EA\partial u_z/\partial z$, the relations between the z-direction displacements and the axial forces at $z = 0$ and L can be obtained as

$$u_{z2}(\omega) = \frac{1}{2}(e^{ik_L L} + e^{-ik_L L})u_{z1}(\omega)$$
$$- \frac{1}{2k_L EAi}(e^{ik_L L} - e^{-ik_L L})N_{zz1}(\omega), \tag{4}$$

$$N_{zz2}(\omega) = -\frac{1}{2}k_L EAi(e^{ik_L L} - e^{-ik_L L})u_{z1}(\omega)$$
$$+ \frac{1}{2}(e^{ik_L L} + e^{-ik_L L})N_{zz1}(\omega), \tag{5}$$

where A is the cross-sectional area. In Eqs. (4) and (5), the axial displacements and forces are the functions of angular frequency and wavenumber. For different dimensions and material properties of a pipe or collar, the modeling parameters, E, A, c_L (or ρ), and L can be modified in Eqs. (4) and (5).
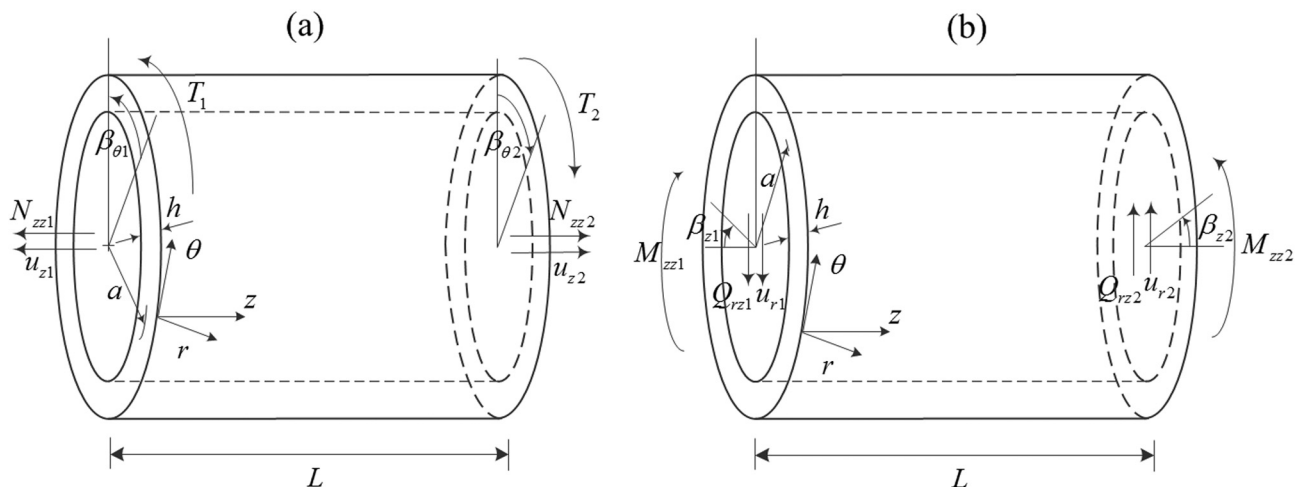

FIG. 1. Vibration variables: (a) Longitudinal and torsional waves and (b) flexural waves.

B. Torsional wave

The torsional wave equation[6] can be expressed as

$$\frac{\partial^2 \beta_\theta}{\partial z^2} = \frac{1}{c_T^2} \frac{\partial^2 \beta_\theta}{\partial t^2},$$

(6)

where β_θ is the torsional angular displacement [see Fig. 1(a)], c_T is the torsional wave speed defined as $c_T = (G/\rho)^{1/2}$, and G is the shear modulus. Similar to the procedure in Sec. II A, by using $T = -J\partial\beta_\theta/\partial z$, the relations between the torsional moments and the angular displacements at $z = 0$ and L can be obtained as

$$\beta_{\theta 2}(\omega) = \frac{1}{2}(e^{ik_T L} + e^{-ik_T L})\beta_{\theta 1}(\omega)$$
$$- \frac{1}{2k_T Ji}(e^{ik_T L} - e^{-ik_T L})T_1(\omega),$$

(7)

$$T_2(\omega) = -\frac{1}{2}k_T Ji(e^{ik_T L} - e^{-ik_T L})\beta_{\theta 1}(\omega)$$
$$+ \frac{1}{2}(e^{ik_T L} + e^{-ik_T L})T_1(\omega),$$

(8)

where J is the torsional rigidity of the system and k_T is the torsional wave number defined as

$$k_T = \frac{\omega}{c_T}.$$

(9)

C. Flexural wave

Based on the Euler-Bernoulli beam theory, the flexural wave equation[7] can be obtained as

$$EI_{FR}\frac{\partial^4 u_r}{\partial z^4} + \rho A \frac{\partial^2 u_r}{\partial t^2} = 0,$$

(10)

where u_r is the transverse displacement [see Fig. 1(b)] and I_{FR} is the area moment of inertia. Then, the relation of the flexural wave variables at $z = 0$ and L is expressed as

$$\begin{bmatrix} u_{r2} \\ \beta_{z2} \\ M_{zz2} \\ Q_{zr2} \end{bmatrix} = \mathbf{A} \begin{bmatrix} u_{r1} \\ \beta_{z1} \\ M_{zz1} \\ Q_{zr1} \end{bmatrix} = \begin{bmatrix} a_{11} & a_{12} & a_{13} & a_{14} \\ a_{21} & a_{22} & a_{23} & a_{24} \\ a_{31} & a_{32} & a_{33} & a_{34} \\ a_{41} & a_{42} & a_{43} & a_{44} \end{bmatrix} \begin{bmatrix} u_{r1} \\ \beta_{z1} \\ M_{zz1} \\ Q_{zr1} \end{bmatrix},$$

(11)

where

$$\beta_z = \frac{\partial u_r}{\partial z},$$

(12)

$$M_{zz} = EI_{FR}\frac{\partial^2 u_r}{\partial z^2},$$

(13)

$$Q_{zr} = -EI_{FR}\frac{\partial^3 u_r}{\partial z^3},$$

(14)

$$a_{11} = \frac{1}{4}(e^{ik_{FR}L} + e^{-ik_{FR}L} + e^{k_{FR}L} + e^{-k_{FR}L}), \quad a_{12} = \frac{1}{4k_{FR}}(-ie^{ik_{FR}L} + ie^{-ik_{FR}L} + e^{k_{FR}L} - e^{-k_{FR}L}),$$

$$a_{13} = \frac{1}{4EI_{FR}k_{FR}^2}(-e^{ik_{FR}L} - e^{-ik_{FR}L} + e^{k_{FR}L} + e^{-k_{FR}L}), \quad a_{14} = \frac{1}{4EI_{FR}k_{FR}^3}(-ie^{ik_{FR}L} + ie^{-ik_{FR}L} - e^{k_{FR}L} + e^{-k_{FR}L}),$$

$$a_{21} = \frac{k_{FR}}{4}(ie^{ik_{FR}L} - ie^{-ik_{FR}L} + e^{k_{FR}L} - e^{-k_{FR}L}), \quad a_{22} = \frac{1}{4}(e^{ik_{FR}L} + e^{-ik_{FR}L} + e^{k_{FR}L} + e^{-k_{FR}L}),$$

$$a_{23} = \frac{1}{4EI_{FR}k_{FR}}(-ie^{ik_{FR}L} + ie^{-ik_{FR}L} + e^{k_{FR}L} - e^{-k_{FR}L}), \quad a_{24} = \frac{1}{4EI_{FR}k_{FR}^2}(e^{ik_{FR}L} + e^{-ik_{FR}L} - e^{k_{FR}L} - e^{-k_{FR}L}),$$

$$a_{31} = \frac{EI_{FR}k_{FR}^2}{4}(-e^{ik_{FR}L} - e^{-ik_{FR}L} + e^{k_{FR}L} + e^{-k_{FR}L}), \quad a_{32} = \frac{EI_{FR}k_{FR}}{4}(ie^{ik_{FR}L} - ie^{-ik_{FR}L} + e^{k_{FR}L} - e^{-k_{FR}L}),$$

$$a_{33} = \frac{1}{4}(e^{ik_{FR}L} + e^{-ik_{FR}L} + e^{k_{FR}L} + e^{-k_{FR}L}), \quad a_{34} = \frac{1}{4k_{FR}}(ie^{ik_{FR}L} - ie^{-ik_{FR}L} - e^{k_{FR}L} + e^{-k_{FR}L}),$$

$$a_{41} = \frac{EI_{FR}k_{FR}^3}{4}(ie^{ik_{FR}L} - ie^{-ik_{FR}L} - e^{k_{FR}L} + e^{-k_{FR}L}), \quad a_{42} = \frac{EI_{FR}k_{FR}^2}{4}(e^{ik_{FR}L} + e^{-ik_{FR}L} - e^{k_{FR}L} - e^{-k_{FR}L}),$$

$$a_{43} = \frac{k_{FR}}{4}(-ie^{ik_{FR}L} + ie^{-ik_{FR}L} - e^{k_{FR}L} + e^{-k_{FR}L}), \quad a_{44} = \frac{1}{4}(e^{ik_{FR}L} + e^{-ik_{FR}L} + e^{k_{FR}L} + e^{-k_{FR}L}),$$

(15)

$$k_{FR} = \left(\frac{\rho A \omega^2}{EI_{FR}}\right)^{1/4}.$$

(16)

D. Vibration transfer matrix

By rewriting Eqs. (4), (5), (7), (8), and (11) in a matrix form, the vibration transfer matrix $\mathbf{T}$ describing the longitudinal, torsional, and flexural wave propagations in the pipe or collar can be obtained as

$$\mathbf{U}_{z=L} = \begin{bmatrix} \mathbf{A} & \vec{\mathbf{0}} \\ \vec{\mathbf{0}} & \mathbf{B} \end{bmatrix} \mathbf{U}_{z=0} = \mathbf{T}\mathbf{U}_{z=0},$$

(17)

where

$$\mathbf{U} = [u_r \ \beta_z \ M_{zz} \ Q_{zr} \ \beta_\theta \ T \ u_z \ N_{zz}]^{\mathrm{T}}, \tag{18}$$

$$\mathbf{B} = \begin{bmatrix} \frac{1}{2}(e^{ik_T L} + e^{-ik_T L}) & -\frac{1}{2k_T Ji}(e^{ik_T L} - e^{-ik_T L}) & 0 & 0 \\ -\frac{1}{2}k_T Ji(e^{ik_T L} - e^{-ik_T L}) & \frac{1}{2}(e^{ik_T L} + e^{-ik_T L}) & 0 & 0 \\ 0 & 0 & \frac{1}{2}(e^{ik_L L} + e^{-ik_L L}) & -\frac{1}{2k_L EAi}(e^{ik_L L} - e^{-ik_L L}) \\ 0 & 0 & -\frac{1}{2}k_L EAi(e^{ik_L L} - e^{-ik_L L}) & \frac{1}{2}(e^{ik_L L} + e^{-ik_L L}) \end{bmatrix}. \tag{19}$$

In Eq. (17), the matrix **A** is defined in Eq. (11).

Since the individual vibration transfer matrix **T** of a single pipe or collar section is a function of its dimensions and material properties regardless of the boundary conditions, the total vibration transfer matrix of a drill pipe system that consists of multiple pipes and collars can be determined by multiplying all of the individual vibration transfer matrices. Therefore, once a measurement is made at one end of the combined drill pipe system, the structural wave variables at the other end can be estimated from the total vibration transfer matrix without making a measurement at this end.

E. Structural damping

The vibration transfer matrix derived in Secs. II A–II D does not include the effects of structural damping. Thus, some wave types in this structural-damping-free system do not decay out, which is physically impossible in reality. In order to include structural damping effects, the "complex" Young's modulus[7] is here defined as

$$\bar{E} = E(1 \pm \eta i), \tag{20}$$

where η is the structural damping coefficient and E is the Young's modulus. The sign of the structural damping depends on the sign convention of the exponential time function, e.g., $\exp(-i\omega t)$. In this article, since $\exp(ikx - i\omega t)$ is defined as the positive-propagating exponential wave component, the negative sign of η in Eq. (20) represents an exponentially-decaying wave component; e.g., the positive sign of η generates an exponentially-increasing wave component as the wave propagates, which is not physically meaningful.

The structural damping coefficient can be calculated by measuring the viscous damping ratio ξ and using the relation between the structural damping coefficient and the viscous damping ratio;[8,9] i.e.,

$$\eta = 2\xi. \tag{21}$$

The viscous damping ratio ξ can be measured by using the half power method.[10]

III. COUPLED VIBRATION TRANSFER MATRIX DERIVED FROM SHELL EQUATIONS

Based on the assumption that the flexural, longitudinal, and torsional wave modes are uncoupled to each other, the

uncoupled vibration transfer matrix is derived from the uncoupled wave equations in Sec. II. However, in a real drill pipe system, these wave modes are coupled due to the pipe's curvature as well as Poisson's ratio. Therefore, the coupling effects are considered to derive an accurate "coupled" vibration transfer matrix in this section. Here, the coupled vibration transfer matrix is proposed to be derived from a "thick" cylindrical shell model.

A. Wave propagation characteristics in a thick cylindrical shell

When the thickness of a cylindrical shell is thin, only three governing equations are needed to describe the vibration motion of a shell in terms of displacements, u_r, u_θ, and u_z.[11,12] For a thick cylindrical shell such as typical drill pipes of which thickness is so thick that shear deformation and rotary inertia cannot be negligible, the rotating angles of β_θ and β_z (see Fig. 1) cannot be expressed in terms of the displacements u_r, u_θ, and u_z. Thus, two additional equations are required to calculate these two rotating angles. The five governing equations[12] to describe the motion of this thick shell structure including the shear deformation and the rotary inertia are expressed as

$$\frac{k'Gh}{a}\frac{\partial \varepsilon_{r\theta}}{\partial \theta} + k'Gh\frac{\partial \varepsilon_{rz}}{\partial z} - \frac{N_{\theta\theta}}{a} - \rho h\frac{\partial^2 u_r}{\partial t^2} = 0, \tag{22}$$

$$\frac{1}{a}\frac{\partial N_{\theta\theta}}{\partial \theta} + \frac{\partial N_{\theta z}}{\partial z} + \frac{k'Gh\varepsilon_{r\theta}}{a} - \rho h\frac{\partial^2 u_\theta}{\partial t^2} = 0, \tag{23}$$

$$\frac{1}{a}\frac{\partial N_{\theta z}}{\partial \theta} + \frac{\partial N_{zz}}{\partial z} - \rho h\frac{\partial^2 u_z}{\partial t^2} = 0, \tag{24}$$

$$\frac{\partial M_{z\theta}}{\partial z} + \frac{1}{a}\frac{\partial M_{\theta\theta}}{\partial \theta} - k'Gh\varepsilon_{r\theta} - \frac{\rho h^3}{12}\frac{\partial^2 \beta_\theta}{\partial t^2} = 0, \tag{25}$$

$$\frac{\partial M_{zz}}{\partial z} + \frac{1}{a}\frac{\partial M_{\theta z}}{\partial \theta} - k'Gh\varepsilon_{rz} - \frac{\rho h^3}{12}\frac{\partial^2 \beta_z}{\partial t^2} = 0, \tag{26}$$

where u is the displacement in the direction denoted by its subscript (see Fig. 1), N_{ij} ($i, j = r, \theta, z$) is the in-plane force (see the appendix for the relation between displacements, forces, and moments), and k' is the shear coefficient. The shear coefficient can be expressed for a circular pipe as[13]

$$k' = \frac{6(1+\mu)\left(1+\left(\frac{r_i}{r_o}\right)^2\right)^2}{(7+6\mu)\left(1+\left(\frac{r_i}{r_o}\right)^2\right)^2+(20+12\mu)\left(\frac{r_i}{r_o}\right)^2},$$

(27)

where r_i and r_o are the inner and outer radii of the circular pipe, respectively, and μ is the Poisson's ratio. Then the assumed wave solutions of Eqs. (22)–(26) for a harmonic excitation can be written as

$$u_r = U_r e^{in\theta} e^{ikz} e^{-i\omega t},$$

(28)

$$u_\theta = U_\theta e^{in\theta} e^{ikz} e^{-i\omega t},$$

(29)

$$u_z = U_z e^{in\theta} e^{ikz} e^{-i\omega t},$$

(30)

$$\beta_\theta = B_\theta e^{in\theta} e^{ikz} e^{-i\omega t},$$

(31)

$$\beta_z = B_z e^{in\theta} e^{ikz} e^{-i\omega t}.$$

(32)

By plugging Eqs. (28)–(32) into Eqs. (22)–(26), an eigenvalue problem can be formulated as

$$\mathbf{Z}\begin{bmatrix} U_r & U_\theta & U_z & B_\theta & B_z \end{bmatrix}^{\mathrm{T}} = \mathbf{0},$$

(33)

where

$$\mathbf{Z}(k,\omega) = \begin{bmatrix} a_1 k^2 + a_2 - \rho h \omega^2 & a_3 & a_4 k & a_5 & a_6 k \\ a_3 & a_7 k^2 + a_8 + \rho h \omega^2 & a_9 k & a_{10} & 0 \\ a_4 k & a_9 k & -Kk^2 + a_{11} + \rho h \omega^2 & 0 & 0 \\ a_5 & a_{10} & 0 & a_{12} k^2 + a_{13} + \frac{\rho h^3}{12}\omega^2 & a_{14} k \\ a_6 k & 0 & 0 & a_{14} k & -Dk^2 + a_{15} + \frac{\rho h^3}{12}\omega^2 \end{bmatrix},$$

(34)

$$a_1 = k'Gh, \quad a_2 = \frac{k'Gh}{a^2}n^2 + \frac{K}{a^2}, \quad a_3 = \frac{k'Gh}{a^2}ni - \frac{K}{a^2}ni, \quad a_4 = \frac{\mu K}{a}i, \quad a_5 = -\frac{k'Gh}{a}n, \quad a_6 = -k'Ghi,$$

$$a_7 = -\frac{K(1-\mu)}{2}, \quad a_8 = -\frac{K}{a^2}n^2 - \frac{k'Gh}{a^2}, \quad a_9 = -\frac{K(1+\mu)}{2a}n, \quad a_{10} = \frac{k'Gh}{a}, \quad a_{11} = -\frac{K(1-\mu)}{2a^2}n^2,$$

$$a_{12} = -\frac{D(1-\mu)}{2}, \quad a_{13} = -\frac{D}{a^2}n^2 - k'Gh, \quad a_{14} = -\frac{D(1+\mu)n}{2a}, \quad \text{and} \quad a_{15} = -n^2\frac{D(1-\mu)}{2a^2} - k'Gh.$$

(35)

For a non-trivial solution, the determinant of the matrix $\mathbf{Z}$ in Eq. (33) should be zero. The latter equation is expressed as a tenth-order polynomial equation and referred to as the characteristic or dispersion equation; i.e.,

$$|\mathbf{Z}(k,\omega)| = 0.$$

(36)

By setting $n=0$ and solving Eq. (36), the dispersion relations (i.e., k-ω relations) for the longitudinal and torsional waves can be obtained as shown in Fig. 2. The material properties of the drill pipe used for Figs. 2–4 are presented in the second column of Table I. At each frequency ω, there are ten roots of k satisfying Eq. (36). When the structural damping is ignored, four of these roots are purely real numbers. These wavenumbers are associated with positive- and negative-going longitudinal and torsional waves depending on the sign and wave speed of each dispersion curve. The positive wavenumbers represent the positive-going waves and the negative wavenumbers, the negative-going waves. The other six complex roots are almost constant independent of frequency and can be ignored due to their extremely large imaginary parts (e.g., $k = \pm 275.8i$, $\pm 48.6 \pm 53.7i$ rad/m): They are exponentially decaying out extremely quickly.

Since the dispersion curves are symmetric with respect to the $k=0$ axis, Fig. 2 shows the only positive wavenumbers. It is shown that in Fig. 2, the dispersion curves obtained from the shell equations are well in line with the uncoupled,
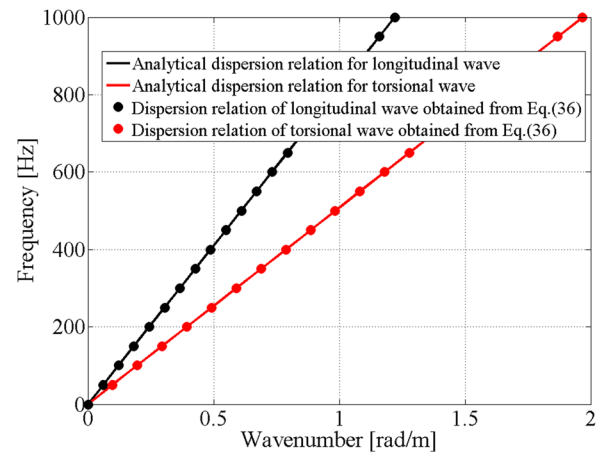

FIG. 2. (Color online) Dispersion relations for $n=0$ longitudinal and torsional wave modes.
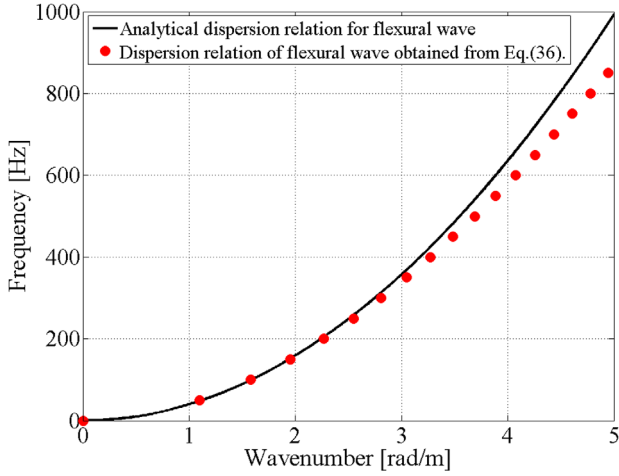
FIG. 3. (Color online) Dispersion relations for $n = 1$ flexural wave mode.

analytical dispersion curves [i.e., $\omega = (E/\rho)^{0.5}k$ and $\omega = (G/\rho)^{0.5}k$]. Thus, it can be concluded that the coupling effects between the longitudinal and torsional waves in the shell model can be ignored in the frequency range up to 1 kHz for the pipe in the second column of Table I.

Similarly, for $n = 1$, the dispersion relation of the flexural wave can be also derived from Eq. (36). In this case, among the ten roots of Eq. (36), two wavenumbers with zero imaginary parts are associated with both positive- and negative-going flexural waves. Here, the only positive wavenumber is plotted in Fig. 3 since the two real wavenumbers are symmetric with respect to the $k = 0$ axis. In addition to the two real wavenumbers, two imaginary wavenumbers with the same magnitude as the real wavenumbers can be obtained that are associated with evanescent flexural waves. The rest six complex roots have large imaginary parts (e.g., $k = \pm 276.1i$, $\pm 46.5 \pm 55.8i$ rad/m) and can be ignored since they are decaying out extremely quickly or increasing exponentially. As shown in Fig. 3, the dispersion curve for the flexural wave obtained by using the shell model is compared with that of the uncoupled, analytical model [i.e., $\omega = (EI/\rho A)^{0.5}k^2$]. In the low frequencies below 200 Hz, the wavenumbers predicted by using the shell model match well with those of the uncoupled, analytical model. As the frequency increases, the discrepancy between the two models
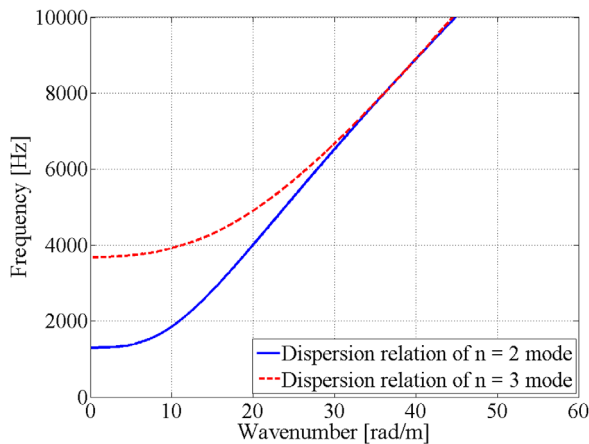

FIG. 4. (Color online) Dispersion relations for $n = 2$ and $n = 3$ modes.

TABLE I. Material properties and diameters of drill pipe system for experimental setup in Fig. 5.

	Pipe	Collar
Young's modulus [Pa]	2.08×10^{11}	
Density [kg/m^3]	7856	
Structural damping coefficient	0.0044	
Poisson's ratio	0.3	
Outer diameter [mm]	73.03	104.78
Inner diameter [mm]	54.65	50.8

increases since the uncoupled, analytical model is valid for only thin beams in low frequencies where the wavelengths are much larger than the cross-sectional dimensions. Since the cut-off frequencies of higher modes (i.e., n is equal to or larger than 2) are higher than 1.3 kHz for the given material properties as shown in Fig. 4, the higher modes are not taken into account in this article.

B. Coupled vibration transfer matrix based on a thick cylindrical shell model

As discussed in Sec. III A, two longitudinal wavenumbers, k_{L+} and k_{L-}, two torsional wavenumbers, k_{T+} and k_{T-}, and four flexural wavenumbers, k_{FR+}, k_{FR-}, k_{FI+}, and k_{FI-} can be obtained from Eq. (36) at a single frequency. These wavenumbers can be referred to as the eigenvalues of the eigenvalue problem in Eq. (33). The corresponding eigenvector, $\mathbf{U} = [U_r\ U_\theta\ U_z\ B_\theta\ B_z]^{\mathrm{T}}$ can then be obtained from Eq. (33) at each frequency and wavenumber. Then, a harmonic wave solution, $\mathbf{u} = [u_r\ u_\theta\ u_z\ \beta_\theta\ \beta_z]^{\mathrm{T}}$ can be expressed by using a superposition of the wave modes represented in terms of the eigenvalues and eigenvectors as

$$
\begin{aligned}
\mathbf{u}(r = a, \theta, z, t) = &[(A^+\mathbf{U}_{FR+}e^{ik_{FR+}z} + A^-\mathbf{U}_{FR-}e^{ik_{FR-}z} \\
&+ B^+\mathbf{U}_{FI+}e^{ik_{FI+}z} + B^-\mathbf{U}_{FI-}e^{ik_{FI-}z})e^{i\theta} \\
&+ C^+\mathbf{U}_{T+}e^{ik_{T+}z} + C^-\mathbf{U}_{T-}e^{ik_{T-}z} \\
&+ D^+\mathbf{U}_{L+}e^{ik_{L+}z} + D^-\mathbf{U}_{L-}e^{ik_{L-}z}]e^{-i\omega t}.
\end{aligned}
\tag{37}
$$

By using the relation[12] of $Q_{zr} = k'hG\varepsilon_{rz}$, the superposition coefficients in Eq. (37) at $z = 0$ can be rewritten in a matrix form as

$$
\mathbf{C}_0 = \mathbf{T}_1^{-1}\mathbf{X}_{z=0},
\tag{38}
$$

where

$$
\mathbf{X} = [u_r\ \beta_z\ M_{zz}\ Q_{rz}\ \beta_\theta\ T\ u_z\ N_{zz}]^{\mathrm{T}},
\tag{39}
$$

$$
\mathbf{C}_0 = [A^+\ A^-\ B^+\ B^-\ C^+\ C^-\ D^+\ D^-]^{\mathrm{T}}.
\tag{40}
$$

When $z = L$, Eq. (37) leads to

$$
\mathbf{X}_{z=L} = \mathbf{T}_1\,\mathbf{T}_2\mathbf{C}_0.
\tag{41}
$$

By plugging Eq. (38) into Eq. (41), the coupled vibration transfer matrix, $\mathbf{T}$ between $z = 0$ and $z = L$ that describes the
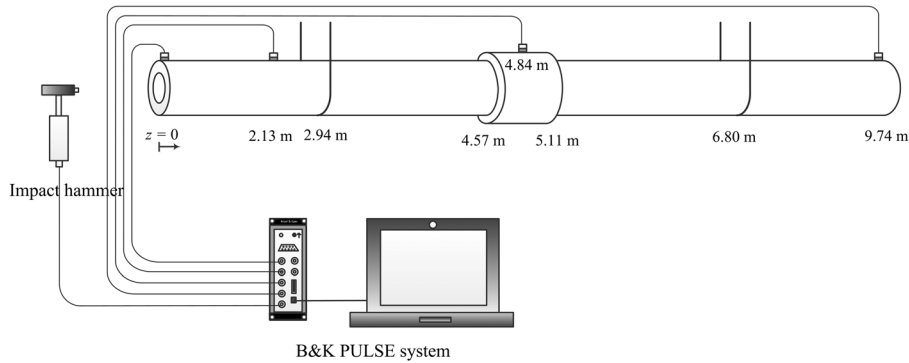
FIG. 5. Experimental setup.

longitudinal, torsional, and flexural waves propagating in the pipe or collar, can be obtained as

$$\mathbf{T} = \mathbf{T}_1\,\mathbf{T}_2\mathbf{T}_1^{-1}. \tag{42}$$

IV. EXPERIMENT AND FE ANALYSES FOR VALIDATION

An experiment and FE analyses are conducted to validate the proposed transfer matrix approaches.

A. Experiments

Figure 5 shows the experimental setup. The material properties and the inner and outer diameters of the drill pipe are presented in Table I. As shown in Fig. 5, the two drill pipe sections, with the same cross-section, which are connected with a collar in the middle, is hanged by using two steel cables at $z = 2.94$ and 6.8 m. These hanging positions are determined arbitrarily with the assumption that these cables are negligibly affecting the vibration responses of the pipe although they actually affect the flexural vibration responses in low frequencies (e.g., below 200 Hz), which will be discussed in Sec. V. A Brüel & Kjær (B&K, Naerum, Denmark) type 8206 impact hammer is used to excite the left end of the drill pipe. Flexural waves are generated by applying a vertical force to the pipe end by using the impact hammer. For an axial impact force to generate longitudinal waves, a circular cover is glued at the left end and the impact hammer is used to excite the center of the circular cover. A B&K PULSE system (Model: 3560-B-130) is used to record acceleration data with a PCB Piezotronics (Buffalo, NY) "triaxial" accelerometer (Model: 356A24). For each axial or transversal excitation case, acceleration data at the four measurement points, $z = 0$, 2.13, 4.84, and 9.75 m as indicated in Fig. 5, are recorded for 8 s at the sampling frequency of 1600 Hz. The measured data at a measurement location include

the three-directional accelerations; i.e., axial, radial (or transversal), and circumferential directions. For each of the axial or transversal excitation, the same measurement is repeated five times. Then, the five spectral data obtained by applying the discrete Fourier transform (DFT) to the acceleration data are linearly averaged to obtain an averaged acceleration spectrum in the axial or transversal direction. Then, the FRFs at the four measurement locations are estimated from the measured acceleration spectra.

Regarding the material properties in Table I, viscous damping coefficients are obtained by applying the half power method[10] [i.e., $\zeta = (\omega_2 - \omega_1)/2\omega_n$, where ω_2 and ω_1 are frequencies at half power points and ω_n is a resonance frequency] to each resonance peak below 300 Hz for the longitudinal and flexural excitation cases at $z = 0, 0.219\,L, 0.5\,L$, and L ($L = 9.74$). The measured damping coefficients are then spatially averaged over all of the measurement locations. Finally, by applying Eq. (21) and averaging over all of the resonance frequencies, the single structural damping coefficient in Table I is obtained. As shown in Table II for the flexural excitation case, although the damping coefficients are slightly frequency-dependent, a frequency-independent structural damping model with the damping value of 0.0044 is used for all of the models in this article otherwise specified. The density in Table I is given by the manufacturer, TSC Drill Pipe, Inc. (Houston, TX). The Young's modulus is determined by optimally fitting the experimental and predicted first natural frequencies (i.e., 278.5 Hz) for the longitudinal excitation case. The estimated value of 208 GPa is close to the Young's modulus of a standard steel (i.e., 30×10^6 psi or 200–210 GPa).

B. Existing experimental data

In addition to conducting the experiments as described in Sec. IV A, the existing experimental data presented in Ref. 1 is also used to validate the proposed transfer matrix approaches. The experimental setup in Ref. 1 is presented in

TABLE II. Resonance peak frequencies and damping coefficients.

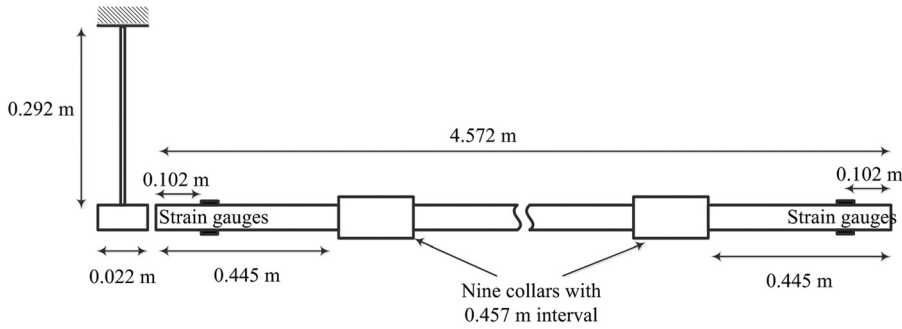|									Structural damping coefficient
Longitudinal excitation case	Resonance frequency [Hz]				278.5				0.0044
	Spatially averaged viscous damping				0.0022				
Flexural excitation case	Resonance frequency [Hz]	31.1	68.4	85.4	109.6	140.4	178.3	256.9	0.0044
	Spatially averaged viscous damping	0.0034	0.0039	0.0016	0.0011	0.0013	0.0023	0.0018	

FIG. 6. Experimental setup in Ref. 1.

Fig. 6. The material properties and geometry information of the scaled drill pipe system in Ref. 1 are listed in Table III. As shown in Fig. 6, the nine copper collars are soldered to the ends of 0.457 m copper pipes and an axial impulse force is generated by dropping the string-suspended mass block. The two sets of two strain gauges are installed at the two axial locations of 0.102 m measured from both ends of the scaled pipe system. These strain gauges are used to record circumferentially symmetric strains (i.e., in-phase, longitudinal strains).

C. Finite element analyses

The results of FE analyses obtained by using a commercial FE software package, ANSYS, are also used to validate the proposed methods. In particular, torsional wave cases are validated only with the FE results since it is difficult to generate pure torsional waves experimentally. The material properties and the inner and outer diameters listed in Table I are used to build a FE model of the pipe system in Fig. 5. The FE model consists of 15 443 nodes and 7871 solid elements of SOLID187. This FE geometry gives the maximum axial space of 0.09 m between two adjacent nodes. Since the maximum frequency of interest is 500 Hz and the slowest wave speed at the maximum frequency is 610 m/s, the maximum space guarantees 13.5 nodes per one wavelength of the slowest wave, which is a sufficiently large number of nodes to obtain an accurate FE result. For the axial, torsional, and transversal excitation, an axial force of 1 N, a torsional moment of 1 N·m, and a vertical force of 1 N are applied at the left-end surface, respectively. By using a harmonic analysis FE solver, acceleration data at the four experimental measurement locations (see Fig. 5) are calculated up to 500 Hz with a 2 Hz frequency resolution. The calculated accelerations are equivalent to FRFs since the unit force or moment is applied as the input.

TABLE III. Material properties and diameters of scaled drill pipe system in Ref. 1.

	Pipe	Collar
Young's Modulus [Pa]	1.18×10^{11}	
Density [kg/m³]	8960	
Outer diameter [mm]	6.4	10.26
Inner diameter [mm]	5.08	6.4
Length [mm]	431.8	25.4

V. RESULTS AND DISCUSSION

Figure 7 shows the experimental, longitudinal strain results presented in Ref. 1 (see also Sec. IV B). The measured results are compared to the temporal strain results obtained by using the uncoupled and coupled transfer matrices. The input forces for the transfer matrix approaches are obtained from the measured strain data at the left measurement location after multiplying EA (i.e., $N_{zz} = EA\partial u_z/\partial z = EA\varepsilon$). Similarly, the output strain data in the transfer matrix approaches at the right measurement location are calculated from the forces obtained from the proposed transfer matrices and divided by EA (i.e., $\varepsilon = \partial u_z/\partial z = N_{zz}/EA$). It is shown that in Fig. 7, the temporal strain results predicted by using both the uncoupled and coupled transfer matrix approaches match well with the measured data. In addition, the results of the two transfer matrix approaches in Fig. 7 are almost identical for this pure longitudinal wave propagation case.

For the "longitudinal" excitation cases described in Fig. 5 and Sec. IV A, the FRFs, in Fig. 8, estimated by using the proposed transfer matrix methods and the ANSYS analyses agree well with the measured FRF results except the valley locations in Figs. 8(a) and 8(b) approximately at 140, 160, and 380 Hz. The measured anti-resonance amplitudes are expected to be inaccurate due to the low signal-to-noise-ratio at these anti-resonance frequencies and the high
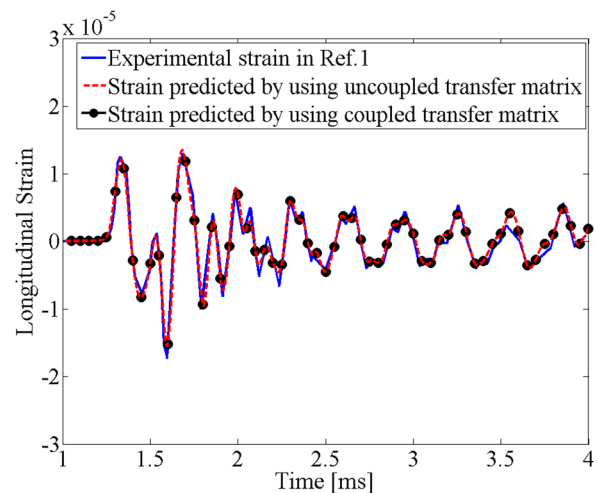

FIG. 7. (Color online) Comparison of longitudinal strain wave data presented in Ref. 1 and obtained by using vibration transfer matrices at strain gauge location in Fig. 7.
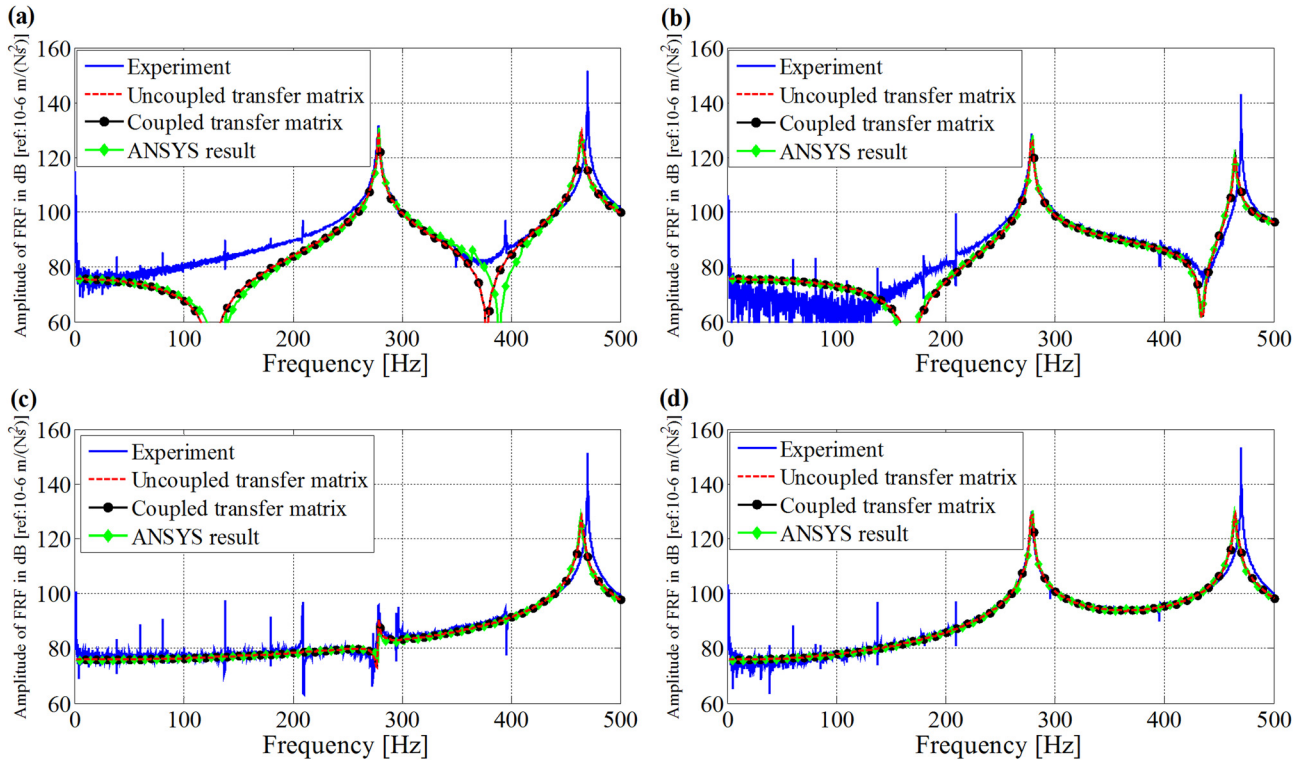
FIG. 8. (Color online) Experimental and predicted FRF results for the case of longitudinal excitation ($L = 9.74$ m): (a) $z = 0$, (b) $z = 0.219\,L$, (c) $z = 0.5\,L$, and (d) $z = L$.

sensitivity of accelerometer placement error on the anti-resonance amplitudes. Although the first resonant amplitude at approximately 280 Hz is consistent throughout all of the results, the second resonant amplitude at approximately 470 Hz is underestimated with all of the predicted results.

This may be caused by the overestimation of the damping value at this second resonance frequency where the resonance amplitude is significantly sensitive to the damping value. In order to investigate this problem in detail, two structural damping coefficients of 0.0044 and 0.00038 are
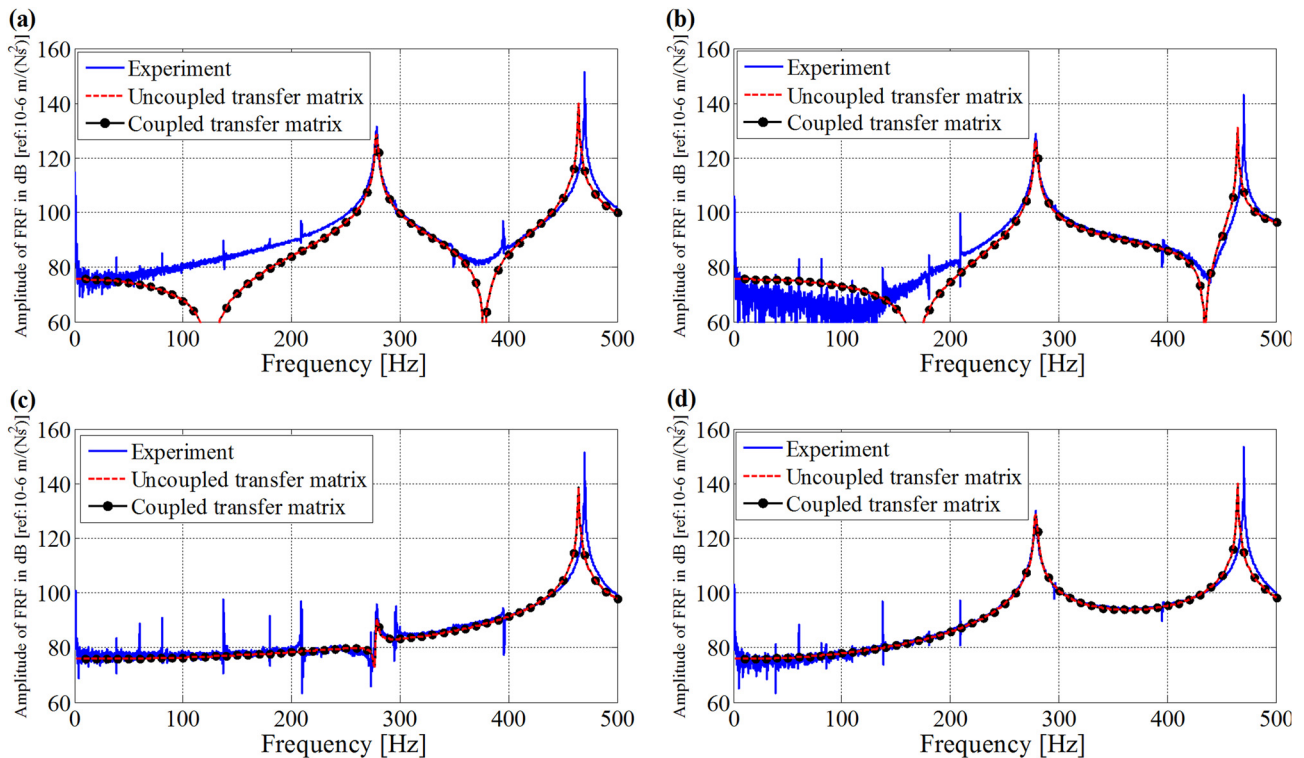

FIG. 9. (Color online) Experimental and predicted FRF results for the case of longitudinal excitation with two different damping coefficients of 0.0044 (from 1 to 370 Hz) and 0.00038 (from 371 to 500 Hz) ($L = 9.74$ m): (a) $z = 0$, (b) $z = 0.219\,L$, (c) $z = 0.5\,L$, and (d) $z = L$.
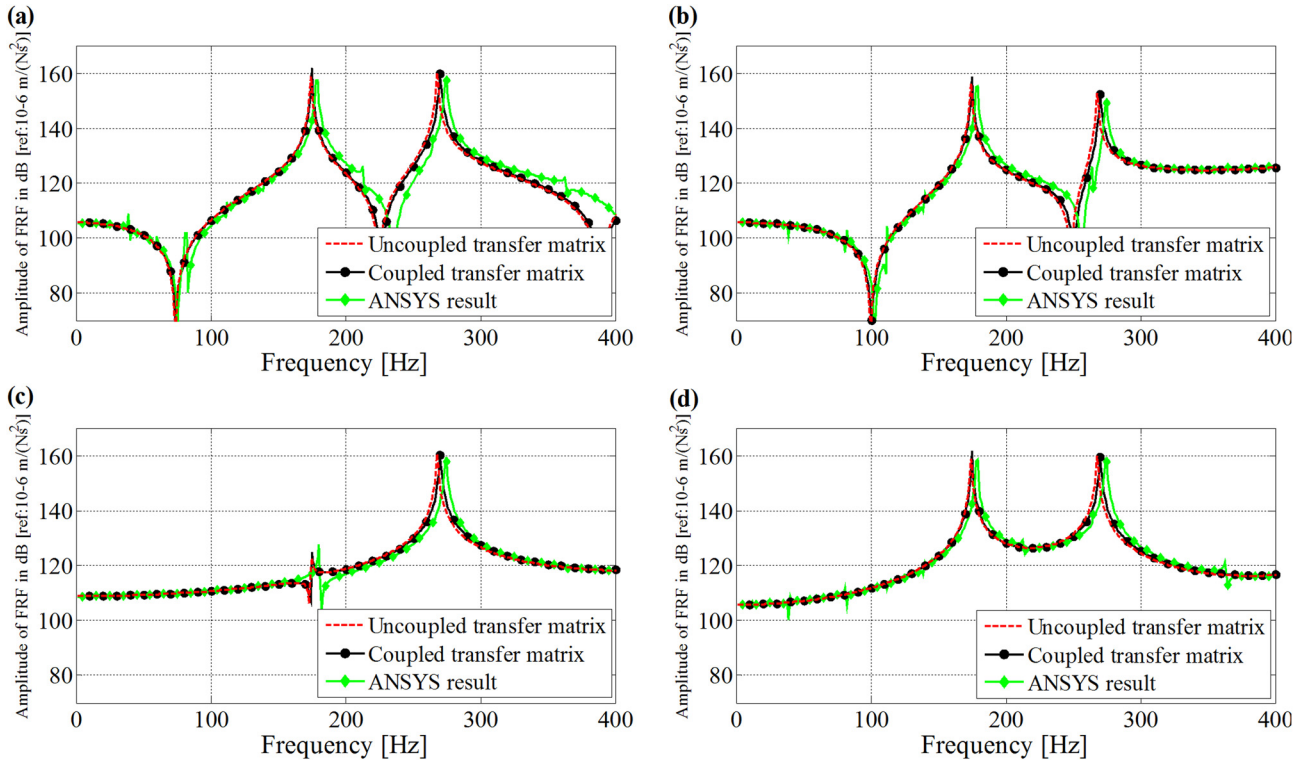
FIG. 10. (Color online) Experimental and predicted FRF results for torsional excitation ($L = 9.74$ m): (a) $z = 0$, (b) $z = 0.219 L$, (c) $z = 0.5 L$, and (d) $z = L$.

applied to two different frequency bands; i.e., the damping coefficient of 0.0044 that is identified by using the half power method at 280 Hz is applied from 1 to 370 Hz and the coefficient of 0.00038 identified at 470 Hz, from 371 to 500 Hz. As shown in Fig. 9, the predicted second resonant amplitudes increase with the smaller damping value, which

make the predicted results more consistent with the experimental results than the constant damping cases in Fig. 8.

For the "torsional" excitation case described in Fig. 5 and Sec. IV C, the FRFs obtained from the proposed transfer matrix methods agree well with the ANSYS analysis results in Fig. 10.
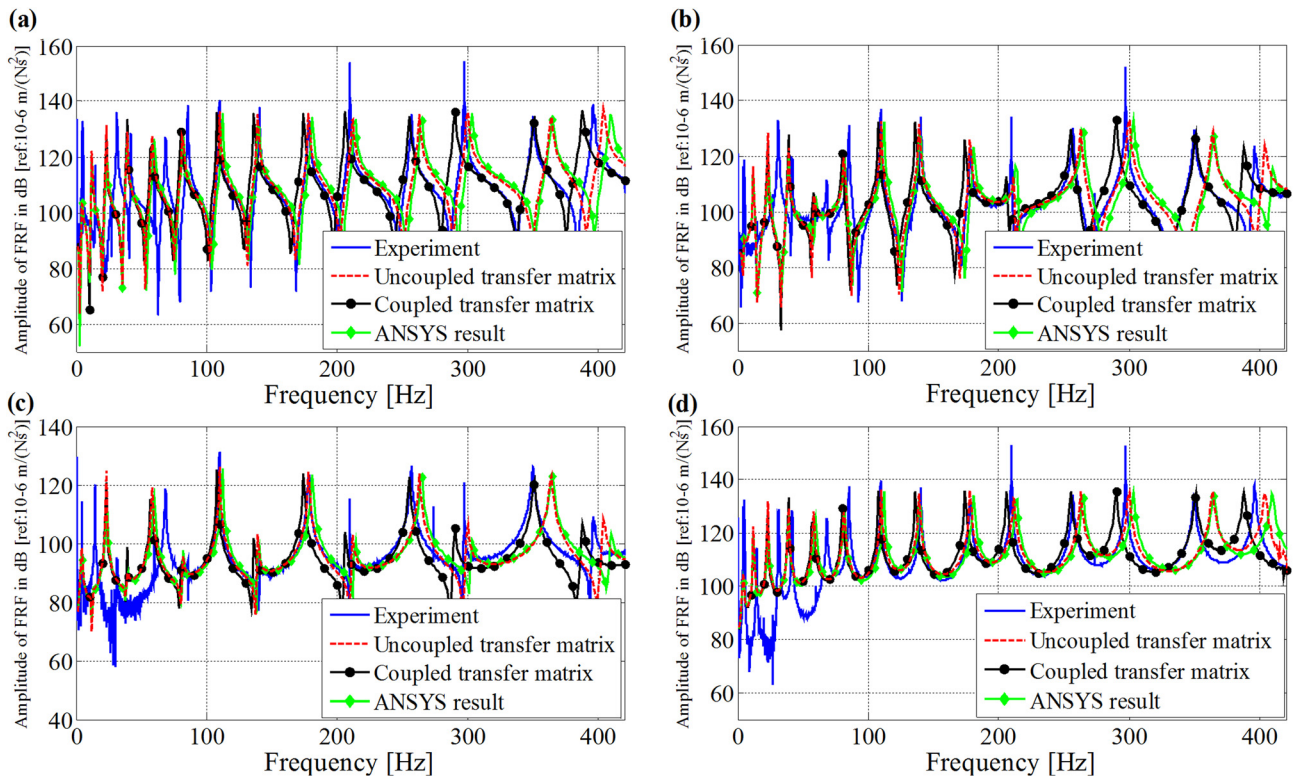

FIG. 11. (Color online) Experimental and predicted FRF results for flexural excitation ($L = 9.74$ m): (a) $z = 0$, (b) $z = 0.219 L$, (c) $z = 0.5 L$, and (d) $z = L$.

TABLE IV. Resonance peak frequencies and frequency differences.

		Resonance frequency [Hz]									Averaged relative error [%]
Longitudinal excitation case	Experiment			279				470			Baseline
	Uncoupled			279				465			0.53
	Coupled			279				465			0.53
	ANSYS			279				464			0.64
Torsional excitation case	ANSYS			179				274			Baseline
	Uncoupled			174				268			2.49
	Coupled			175				270			1.84
Flexural excitation case	Experiment	110	140	178	209	257	297	350	396	457	Baseline
	Uncoupled	111	139	178	212	263	300	364	404	481	1.96
	Coupled	108	136	174	206	255	290	351	388	460	1.61
	ANSYS	112	139	181	214	264	303	365	409	478	2.61

For the "flexural" excitation case in Fig. 11, at low frequencies (e.g., below 100 Hz), the boundary condition in the experiment cannot be assumed as a free-free boundary condition since the drill pipe is hanged by the two steel cables as shown in Fig. 5, while the predicted results are based on the free-free boundary condition. Therefore, there are some discrepancies between the measured and predicted results in the low frequencies. However, above 100 Hz, the discrepancies become negligible, resulting in the predicted FRF results matched well with the measured results. As shown in Fig. 3, as the frequency increases, the analytical solution based on the Bernoulli-Euler beam theory results in lower wavenumbers (i.e., higher stiffness) than the thick-shell model. Therefore, the resonance frequencies estimated by using the analytical, uncoupled approach are higher than those of the thick-shell-theory-based, coupled transfer matrix and experimental approaches in Fig. 11. At high frequencies above 250 Hz, the FRFs predicted from the coupled vibration transfer matrix are better fitted to the measured results than those from the uncoupled vibration transfer matrix.

For the purpose of evaluating the performance of each modeling approach, Table IV presents resonance peak frequencies and relative errors of the predicted results from the baseline frequencies. It is shown that in general, the coupled transfer approach has the minimum relative error. It is noteworthy that the coupled vibration transfer matrix approach with the 1.84% relative error generates more closely matched torsional results to the ANSYS results than the uncoupled method with the 2.49% relative error. For the flexural excitation case, the uncoupled vibration transfer matrix approach results in the better matched results to the measured results with the 1.61% relative error than the other two approaches with the relative errors of 1.96% and 2.61%.

As shown in the flexural excitation case of Table IV, the ANSYS model slightly overestimates the natural frequencies systematically. For the purpose of investigating the potential

TABLE V. Estimated resonance peak frequencies according to number of node in ANSYS.

	# of nodes	Resonance frequency [Hz]									Averaged relative error [%]
Longitudinal excitation case	Experiment			279				470			Baseline
	5372			279				471			0.11
	9774			278				467			0.50
	15443			279				464			0.64
	18399			274				485			2.49
	66958			275				485			2.31
Torsional excitation case	Experiment			179				274			Baseline
	5372			197				307			11.05
	9774			182				282			2.30
	15443			179				275			0.18
	18399			183				289			3.85
	66958			174				277			1.94
Flexural excitation case	Experiment	110	140	178	209	257	297	350	396	457	Baseline
	5372	91	127	164	213	268	325	392	483	-	N/A
	9774	113	141	183	216	269	307	370	415	487	3.86
	15443	112	139	181	214	264	303	365	409	478	2.61
	18399	107	134	172	204	251	289	345	388	451	2.51
	66958	106	133	170	202	248	285	340	382	446	3.64

Han et al.: Wave propagation models in drill strings

stiffening effects of the FE model with an insufficient number of nodes, a convergence test is performed by increasing the number of nodes. As shown in Table V, the ANSYS model becomes softer as the number of nodes increases, in particular, for the flexural excitation case in high resonance frequencies. Based on all of the results in Table V, the total node number of 15 443 is selected as an optimal node number in terms of computational accuracy and efficiency to generate all of the ANSYS prediction results in this article.

VI. CONCLUSION

In this paper, the uncoupled and coupled vibration transfer matrices are derived in order to analytically estimate the longitudinal, torsional, and flexural waves propagating through long drill strings in a computationally-efficient way. The uncoupled transfer matrix is here derived from the three uncoupled wave equations. Since the wave modes are weakly coupled in reality, the vibration transfer matrix including the coupling effects is derived from the thick circular cylindrical shell model. The proposed methods are validated experimentally and numerically. Through the comparison between the measured and predicated results, it is shown that the simplistic uncoupled transfer matrix approach can be used to accurately predict the critical vibrations of a drill pipe system such as stick-slip and bit-bounce below 500 Hz for the drill strings considered in this article, although the coupled transfer matrix approach can generate better results than the uncoupled transfer matrix approach, in particular, for estimating the torsional and flexural vibration.

APPENDIX: RELATION BETWEEN DISPLACEMENTS, FORCES, AND MOMENTS

The in-plan force, N and the moment, M in Eqs. (22)–(26) are represented as

$$N_{\theta\theta} = K(\varepsilon_{\theta\theta}^0 + \mu\varepsilon_{zz}^0), \quad N_{zz} = K(\varepsilon_{zz}^0 + \mu\varepsilon_{\theta\theta}^0),$$
$$N_{\theta z} = \frac{K(1-\mu)}{2}\varepsilon_{\theta z}^0, \tag{A1}$$

$$M_{\theta\theta} = D(k_{\theta\theta} + \mu k_{zz}), \quad M_{zz} = D(k_{zz} + \mu k_{\theta\theta}),$$
$$M_{\theta z} = \frac{D(1-\mu)}{2}k_{\theta z}, \tag{A2}$$

where the membrane strains and the curvatures are defined as

$$\varepsilon_{\theta\theta}^0 = \frac{1}{a}\frac{\partial u_\theta}{\partial \theta} + \frac{u_r}{a}, \quad \varepsilon_{zz}^0 = \frac{\partial u_z}{\partial z}, \quad \varepsilon_{\theta z}^0 = \frac{1}{a}\frac{\partial u_z}{\partial \theta} + \frac{\partial u_\theta}{\partial z}, \tag{A3}$$

$$\varepsilon_{r\theta} = \frac{1}{a}\frac{\partial u_r}{\partial \theta} - \frac{u_\theta}{a} + \beta_\theta, \quad \varepsilon_{rz} = \frac{\partial u_r}{\partial z} + \beta_z, \tag{A4}$$

$$k_{\theta\theta} = \frac{1}{a}\frac{\partial \beta_\theta}{\partial \theta}, \quad k_{zz} = \frac{\partial \beta_z}{\partial z}, \quad k_{\theta z} = \frac{1}{a}\frac{\partial \beta_z}{\partial \theta} + \frac{\partial \beta_\theta}{\partial z}. \tag{A5}$$

In Eqs. (A1) and (A2), K and D is the membrane stiffness and the bending stiffness defined as

$$D = \frac{Eh^3}{12(1-\mu^2)}, \tag{A6}$$

$$K = \frac{Eh}{1-\mu^2}, \tag{A7}$$

where μ and h are Poisson's ratio and thickness, respectively.

[1] D. S. Drumheller, "Acoustical properties of drill strings," J. Acoust. Soc. Am. **85**, 1048–1064 (1989).
[2] C. Y. Wang, W. X. Qiao, and W. Q. Zhang, "Using transfer matrix method to study the acoustic property of drill strings," *IEEE International Symposium on Signal Processing and Information Technology*, Waterloo, Canada (2006), pp. 415–419.
[3] E. Kreuzer and M. Steidl, "Controlling torsional vibrations of drill strings via decomposition of traveling waves," Arch. Appl. Mech. **82**, 515–531 (2012).
[4] K. S. Peat, "A transfer matrix for an absorption silencer element," J. Sound Vib. **146**, 353–360 (1991).
[5] B. H. Song and J. S. Bolton, "A transfer matrix approach for estimating the characteristic impedance and wave numbers of limp and rigid porous materials," J. Acoust. Soc. Am. **107**, 1131–1152 (2000).
[6] K. F. Graff, *Wave Motion in Elastic Solids* (Dover Publications, Mineola, NY, 1991), pp. 75–77, 125–126, and 140–143.
[7] F. Fahy, *Sound and Structural Vibration* (Academic Press, San Diego, CA, 1987), pp. 42–51.
[8] A. M. Horr and L. C. Schmidt, "Modeling of nonlinear damping characteristics of a viscoelastic structural damper," Eng. Struct. **18**, 154–161 (1996).
[9] ASTM Standard E756-05, Standard test method for measuring vibration-damping properties of materials (ASTM International, 2010).
[10] L. Meirovitch, *Elements of Vibration Analysis*, 2nd ed. (McGraw-Hill, New York, 1986), pp. 50–55.
[11] Y.-J. Kim and J. S. Bolton, "Effects of rotation on the dynamics of a circular cylindrical shell with application to tire vibration," J. Sound Vib. **275**, 605–621 (2004).
[12] W. Soedel, *Vibrations of Shells and Plates*, 3rd ed. (Marcel Dekker, Inc., New York, 2004), pp. 322–336.
[13] G. Cowper, "The shear coefficient in Timoshenko's beam theory," J. Appl. Mech. **33**, 335–340 (1966).